Collisional ionization and excitation of H_2: Dependence on the orientation of the internuclear axis

A. K. Edwards, R. M. Wood, and M. A. Mangan
Department of Physics and Astronomy, University of Georgia, Athens, Georgia 30602

R. L. Ezell
Department of Chemistry and Physics, Augusta College, Augusta, Georgia 30910
(Received 17 June 1992)

The cross sections for the double ionization, ionization plus excitation, and double excitation of H_2 by protons and electrons have been measured as a function of the angle between the internuclear axis of the target and the projectile-beam direction. Measurements are reported for angles ranging from 18° to 90° and projectile-beam energies of 0.75, 1.0, and 2.0 MeV/amu. Simple model calculations predict a different angular dependence depending on whether the final configuration of a particular reaction channel is or is not dipole allowed. Comparison is made between prediction and measurement. For both electron and proton projectiles, the sum of the yield in all channels follows the form corresponding to a dipole-allowed final state. Some individual channels do not.

PACS number(s): 34.50.Gb, 34.90.+q, 34.80.Gs

I. INTRODUCTION

For approximately ten years now, a concentrated study has been made on the study of two-electron processes in fast collisions of ions with helium [1–11]. These processes include double ionization, ionization plus excitation, and double excitation. In the case of double ionization it was found that electrons have about twice the cross section as that of equivelocity protons in the region of collision velocities of about 5 a.u. Subsequent studies with antiprotons and positrons showed that this effect was dependent on projectile charge rather than mass [5,7,8]. Similar measurements have been made more recently on the double excitation [9,11] and on the ionization plus excitation [10] of helium. The factor-of-2 cross-section ratio was found to hold in the latter case but not in the double-excitation process.

Several different theoretical approaches [12–17] have been used to explain these results. Most discussions have centered on the arguments of McGuire [12,13] which state that the factor of 2 is due to an interference between first and second Born terms in the collision. In the first Born term, a single projectile–target-electron interaction occurs followed by an electron-electron or electron-hole interaction. In the literature, these interactions have been referred to, respectively, as TS1 (two-step 1) and shakeoff or shakeup. The second Born term is the double-collision process consisting of two projectile-electron interactions and is known as TS2. The interference of the two Born amplitudes produces a Z^3 term in the Born series. Originally [12], these arguments were used to explain double-ionization measurements and the only first Born process considered was shakeoff. Becker [13] raised the objection that the first Born term would lead to an *sp* final state while the second Born contribution would be a *pp* state and hence there would be no interference. The calculations of Reading and Ford [15] removed the inconsistency between the arguments of McGuire and Becker by showing the necessity of a nondipole contribution to the collision in order for interference to occur. This might be, for example, a double-collision process leading to an *sp* final state. These points are discussed further in Sec. III.

More recently, discussions have centered around the relative phase of the first and second Born terms, the emphasis being on whether or not the second Born term has real or imaginary parts to mix with the first Born term which can be either purely real or purely imaginary. McGuire and Straton [18] have shown that mixing of the first and second Born terms occurs from time-ordering effects which are related to off-shell virtual intermediate states. Stolterfoht [19] has discussed these phase relations and pointed out their effects in the double excitation

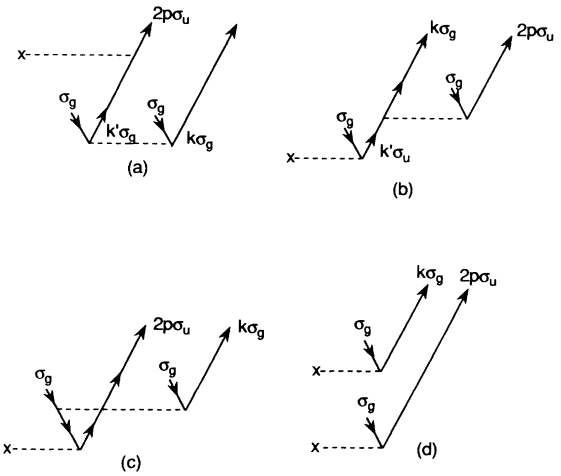

FIG. 1. Goldstone diagrams for (a) a single projectile-electron interaction preceded by an electron-electron interaction; (b) and (c) single projectile-electron interaction followed by an electron-electron or electron-hole interaction; and (d) a double-collision process in which there are two projectile-electron interactions which lead to the final state.

of helium and Li-like ions.

All of the work mentioned above has been concerned with the two-electron system of helium, but the interference effect leading to the enhanced cross section for electron bombardment has also been observed experimentally [20–22] in collisions with an H_2 target. Unlike the helium target, however, the factor of 2 has been observed [21] in double excitation of H_2. (Whether or not the factor of 2 should be present in the double excitation of helium is still an open question [18,23].) The previous measurements [20,21] on H_2 were done on molecules that had their internuclear axis oriented perpendicular to the beam axis. This article reports on the cross sections for two-electron processes in H_2 for other orientations of the internuclear axis. Based on the analysis given in Sec. III these angular measurements yield information on the relative contributions from dipole and nondipole interactions in the collision.

II. EXPERIMENTAL PROCEDURES

The cross sections reported in this work were measured using a time-energy spectroscopy (TES) technique which has been described in detail elsewhere [21]. A beam of electrons from an electron gun or a beam of protons from a Van de Graaff accelerator was passed through a differentially pumped target region containing hydrogen gas at a pressure of 1.3×10^{-4} Torr. Care was taken to ensure that the proton and electron beams followed exactly the same path and had the same spatial profile.

The intent of the experimental technique was to measure the yield of H^+ ions with energies in the range from 1 to 15 eV, which were produced in the collision-induced dissociation of H_2 target molecules. The energies of H^+ ions were measured with a hemispherical analyzer, which was positioned in the reaction plane at angles ranging from 18° to 90° with respect to the direction of the incident projectile beam. The analyzer subtended a solid angle of 3.05×10^{-3} sr and a planar angle of 2.3°.

The TES technique involves the measurement of the time of flight (TOF) and energy of ions emitted by the target as the result of the collision. In this experiment the TOF measurement allowed separation of the H^+ ions of interest from other contaminant ions. The energy

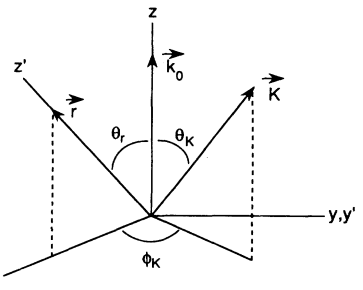

FIG. 2. The z axis of the unprimed system is defined by the projectile direction. The z' axis of the primed system is defined by the molecular axis which lies in the xz plane. The x' axis is not shown.

TABLE I. Basis functions $Y_{lm}(\hat{\mathbf{q}})$ used for $g(\hat{\mathbf{q}})$ in the wave function $\psi_{i,f}$.

State	$g(q)$
σ_g	Y_{00}
σ_u	Y_{10}
π_u	Y_{11} or Y_{1-1}

scale of the hemispherical analyzer was calibrated using several different targets which produced ion peaks of known energies.

In interpreting the angular distributions, the axial recoil approximation [24] was assumed to apply. That is, it was assumed that the target molecular ion formed in the collision would dissociate along the line defined by the molecule's internuclear axis. This should be the case since collision times are much shorter than dissociation times, which are in turn much shorter than molecular rotation times. Hence, with the analyzer set at an angle of 18°, the observed H^+ ions were produced by target molecules whose internuclear axes made angles of 18° with the beam direction. Absolute cross sections were not measured in this work. Instead, the cross sections reported here were normalized to the earlier measurements at 90° [21].

The first step in the reduction of the raw data obtained

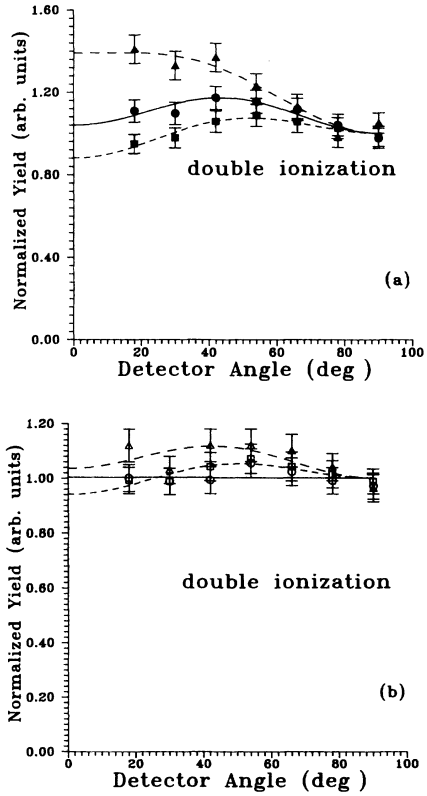

FIG. 3. Yield of H^+ ions from the doubly ionized state of H_2 as a function of the orientation of the molecular axis relative to the beam direction. (a) electrons at 408 eV (●), 154 eV (▲), and 1089 eV (■); (b) protons at 0.75 MeV (○), 1.0 MeV (△), and 2.0 MeV (□). The smooth line is a fit to the data (see Table IV). The yields have been normalized at 90°.

TABLE II. Values of the coefficients A and B of Eq. (5) and the reduced χ^2.

	Electrons					
	0.75 MeV/amu		1 MeV/amu		2 MeV/amu	
State	A	B	A	B	A	B
$2p\pi_u$	−0.04±0.21	−0.20±0.22	0.29±0.22	−0.48±0.24	1.14±0.25	−1.17±0.28
χ^2	0.30		0.14		1.0	
H^+H^+	0.65±0.24	−0.61±0.27	0.83±0.27	−0.44±0.24	0.39±0.23	−0.51±0.25
χ^2	0.34		0.78		0.15	
Dbly exc						
	Protons					
	0.75 MeV/amu		1 MeV/amu		2 MeV/amu	
State	A	B	A	B	A	B
$2p\pi_u$	1.03±0.27	−0.82±0.29	0.35±0.23	−0.50±0.25	0.59±0.24	−0.68±0.26
χ^2	4.7		3.4		1.8	
H^+H^+	0.17±0.23	−0.19±0.25	0.43±0.24	−0.39±0.27	0.26±0.23	−0.32±0.25
χ^2	0.28		0.94		0.16	
Dbly exc	−1.16±0.17	0.71±0.17	−0.76±0.17	0.29±0.18	−1.15±0.17	0.84±0.18
χ^2	2.3		0.32		1.2	

at any given angle is a graph of the yield of H^+ ions as a function of ion energy. As in our earlier work [21], it was assumed that five reaction channels dominate the yield above 1 eV. Three of these are ionization-plus-excitation channels involving repulsive states of H_2^+: $2p\sigma_u$, $2p\pi_u$, and $2s\sigma_g$. One channel is the double-ionization channel and the last is a representation of double-excitation contributions which cannot be attributed to any single molecular state.

After various corrections are made to the raw data, the yield attributed to each of the five reaction channels just identified is determined. These yields are reduced to cross sections in the usual manner. The reader is referred to the paper describing the measurements at 90° for a detailed discussion [21].

III. THEORY

The Goldstone diagrams shown in Fig. 1 illustrate the interactions of concern. In Fig. 1(a) there is a single projectile-electron interaction preceded by an electron-electron interaction. In Figs. 1(b) and 1(c) there is a single projectile-electron interaction followed by an electron-electron or electron-hole interaction. Figure 1(d) depicts the double-collision process in which there are two projectile-electron interactions which lead to the final state. Any dependence of the cross sections on the orientation of the internuclear axis relative to the beam direction is expressed in the matrix element for the excitation by the projectile-electron interaction. The matrix elements for the electron-electron interaction are independent of the projectile coordinates.

The transition moment for the beam interaction can be written in terms of the single-electron matrix element

$$T_{if}=\langle \psi_f | V | \psi_i \rangle \ , \tag{1}$$

where V is the Coulomb interaction between the charged projectile and a target electron. The direct product of the irreducible representations of each term of T_{if} must contain the totally symmetric irreducible representation in order for T_{if} not to vanish. For example, if the initial-state wave function ψ_i has σ_g symmetry and the final-state wave function ψ_f has σ_u symmetry in the $D_{\infty h}$ group, then the irreducible representation of V must also be σ_u in order for the direct product to yield σ_g. For the processes shown in Figs. 1(b)–1(d) the initial-state wave function has $1s\sigma_g$ symmetry. For the ground-state correlation process indicated by Fig. 1(a) the initial state of the electron to be used in Eq. (1) is considered to be either σ_g, σ_u, or π_u. The final state of the electron after the beam interaction in all four processes is considered to be either σ_g (s wave for the ejected electron), or σ_u or π_u (p wave for the ejected electron). With these initial- and final-state wave functions, it is possible to pick out the symmetries of the interaction potential and then, within

TABLE III. Values of the coefficient A of Eq. (4) and the reduced χ^2.

	0.75 MeV/amu		1 MeV/amu		2 MeV/amu	
State	Electrons	Protons	Electrons	Protons	Electrons	Protons
$2s\sigma_g$	−0.10±0.06	−0.28±0.05	0.14±0.06	−0.26±0.05	−0.05±0.06	−0.13±0.05
χ^2	0.22	0.68	1.8	2.7	0.12	0.26
$2p\sigma_u$	−0.39±0.05	−0.20±0.05	−0.49±0.05	−0.24±0.05	−0.63±0.04	−0.35±0.05
χ^2	0.13	0.56	0.12	0.30	0.24	0.07
Dbly exc	−0.27±0.05		−0.43±0.05		−0.46±0.05	
χ^2	0.39		0.44		1.2	

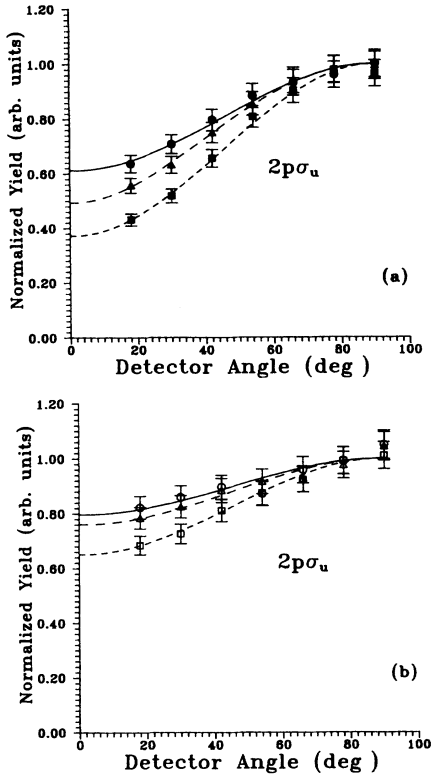

FIG. 4. Yield of H^+ ions from the $2p\sigma_u$ state of H_2 as a function of the orientation of the molecular axis relative to the projectile direction. (a) electrons at 408 eV (●), 545 eV (▲), and 1089 eV (■); (b) protons at 0.75 MeV (○), 1.0 MeV (△), and 2.0 MeV (□). The smooth line is a fit to the data (see Table IV). The yields have been normalized at 90°.

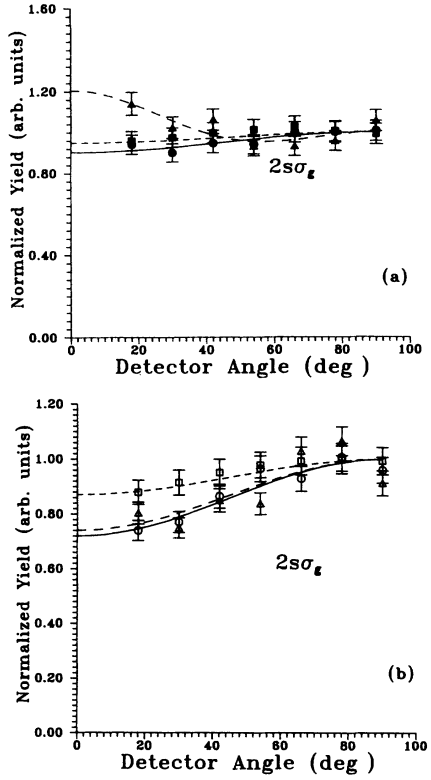

FIG. 5. Yield of H^+ ions from the $2s\sigma_g$ state of H_2 as a function of the orientation of the molecular axis relative to the projectile direction. (a) electrons at 408 eV (●), 545 eV (▲), and 1089 eV (■); (b) protons at 0.75 MeV (○), 1.0 MeV (△), and 2.0 MeV (□). The smooth line is a fit to the data (see Table IV). The yields have been normalized at 90°.

the confines of the first Born approximation, it is possible to discuss orientation effects.

That part of the transition moment which deals with the orientation of the internuclear axis can be expressed [25] in first Born as

$$T_{if} \sim \int\int d\mathbf{r}\, d\mathbf{q}\, \psi_f^* e^{i\mathbf{K}\cdot\mathbf{q}} \psi_i \ , \tag{2}$$

where $\mathbf{K}=\mathbf{k}_0-\mathbf{k}$ is the momentum transfer, $\mathbf{k}_0$ and $\mathbf{k}$ are the initial and final momenta of the projectile, respectively, $\mathbf{q}$ is the position of the target electron relative to the center of the molecule, and $\mathbf{r}$ denotes the orientation and magnitude of the internuclear axis.

The symmetries of the wave functions are defined relative to a molecule-fixed coordinate system. Let this system be denoted as the primed coordinate system with the z' axis along $\mathbf{r}$, and let the unprimed system be a laboratory-fixed coordinate system with the z axis along the beam direction $\mathbf{k}_0$ as shown in Fig. 2. As stated earlier, the axial recoil approximation is assumed to hold and the molecular axis is considered fixed during the entire collision and dissociation process.

TABLE IV. The general behavior of the cross section for the specified final state on the orientation of the internuclear axis relative to the beam direction.

Projectile	$1+A\cos^2\theta_r$	$1+A\cos^2\theta_r+B\cos^4\theta_r$
H^+	$2p\sigma_u$	$2p\pi_u$
	$2s\sigma_g$	H^+H^+
		Doubly excited
e^-	$2p\sigma_u$	$2p\pi_u$
	$2s\sigma_g$	H^+H^+
	Doubly excited	

The primed coordinate system, i.e., the molecular orientation, is specified by the polar angles (θ_r,ϕ_r) of $\mathbf{r}$ relative to $\mathbf{k}_0$. The x axis is chosen so that $\phi_r=0$. The set of polar angles $(\theta_r,0)$ is also the position of the detector relative to the beam direction.

In the primed system the wave functions must have the symmetries of the initial and final states and are written as

$$\psi_{i,f}=f_{i,f}(q)g_{i,f}(\hat{\mathbf{q}})\chi_{i,f}(r) \ ,$$

where spherical harmonics are used for $g_{i,f}(\hat{\mathbf{q}})$ and serve as the basis functions for the irreducible representations of the molecular states. The forms of $g_{i,f}(\hat{\mathbf{q}})$ used here are listed in Table I. The vibrational part of the wave function is given by $\chi_{i,f}(r)$.

The function of $e^{i\mathbf{K}\cdot\mathbf{q}}$ can be written [26] in the primed

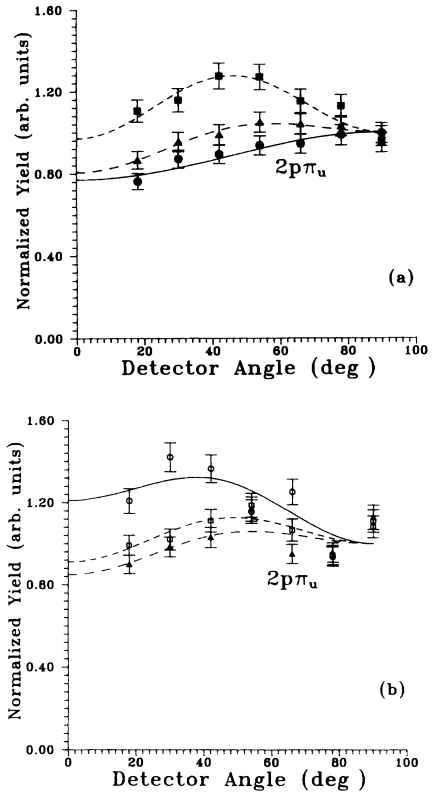

FIG. 6. Yield of H^+ ions from the $2p\pi_u$ state of H_2 as a function of the orientation of the molecular axis relative to the projectile direction. (a) electrons at 408 eV (●), 545 eV (▲), and 1089 eV (■); (b) protons at 0.75 MeV (○), 1.0 MeV (△), and 2.0 MeV (□). The smooth line is a fit to the data (see Table IV). The yields have been normalized at 90°.

system as

$$e^{i\mathbf{K}\cdot\mathbf{q}}=4\pi\sum_{l,m} i^l j_l(kq)Y_{l,m}(\hat{\mathbf{q}})Y^*_{l,m}(\hat{\mathbf{K}}') ,$$

where $\hat{\mathbf{K}}'$ notes the orientation of $\mathbf{K}$ relative to $\mathbf{r}$. Only those partial waves of the proper symmetry can contribute to T_{if} of Eqs. (1) and (2) for specified initial and final states. For initial and final states $l_i m_i$ and $l_f m_f$ the transition moment becomes

$$\begin{aligned} T_{if} &\sim \int d\hat{\mathbf{q}} \sum_{l,m} g_f^*(\hat{\mathbf{q}})Y_{l,m}(\hat{\mathbf{q}})g_i(\hat{\mathbf{q}})Y^*_{l,m}(\hat{\mathbf{K}}') , \\ T_{if} &\sim \sum_{l,m}(-1)^{m_f}\left[\frac{(2l_f+1)(2l+1)(2l_i+1)}{4\pi}\right]^{1/2} \\ &\quad\times\begin{pmatrix} l_f & l & l_i \\ -m_f & m & m_i\end{pmatrix}\begin{pmatrix} l_f & l & l_i \\ 0 & 0 & 0\end{pmatrix} Y^*_{lm}(\hat{\mathbf{K}}') , \end{aligned} \tag{3}$$

where l satisfies the triangular condition $\Delta(l_f l l_i)$ and $l_f+l+l_i=$ even integer, and $m=m_f-m_i$. Only terms involved with the orientation of the molecular axis have been kept.

This result is in terms of the primed system and the angle between $\mathbf{K}$ and $\mathbf{r}$. To analyze experimental data, one needs an expression in terms of the angles between $\mathbf{r}$ and $\mathbf{k}_0$ and between $\mathbf{K}$ and $\mathbf{k}_0$. This is found by changing $Y^*_{lm}(\hat{\mathbf{K}}')$ to $Y_{lm}(\hat{\mathbf{K}}')$ and then using the rotation matrices,

$$Y_{lm}(\hat{\mathbf{K}}')=\sum_{m'} Y_{lm'}(\hat{\mathbf{K}})D^l_{m'm}(0,-\theta_r,0) ,$$

where $\hat{\mathbf{K}}$ specifies the orientation of $\mathbf{K}$ relative to $\mathbf{k}_0$ and θ_r is the angle between $\mathbf{r}$ and $\mathbf{k}_0$.

For the double-collision process the interaction is expressed as the product of two matrix elements, one for each interaction, and each similar to Eq. (2). For a specified final configuration the amplitudes for the single-collision events are added to those for the double-collision events and the sum squared and integrated over the azimuthal angle ϕ_K.

If the final configuration is dipole allowed, e.g., a $1s\sigma_g^2\rightarrow 2p\sigma_u k\sigma_g$ transition, then the cross section is of the form

$$\sigma=\sigma_0(K)[1+A(\theta_K)\cos^2\theta_r] . \tag{4}$$

The nondipole contribution to the interaction occurs in the double-collision process. If the final configuration is nondipole allowed, e.g., a $1s\sigma_g^2\rightarrow 2p\sigma_u k\sigma_u$ transition, then the cross section is of the form

$$\sigma=\sigma_0(K)[1+A(\theta_K)\cos^2\theta_r+B(\theta_K)\cos^4\theta_r] . \tag{5}$$

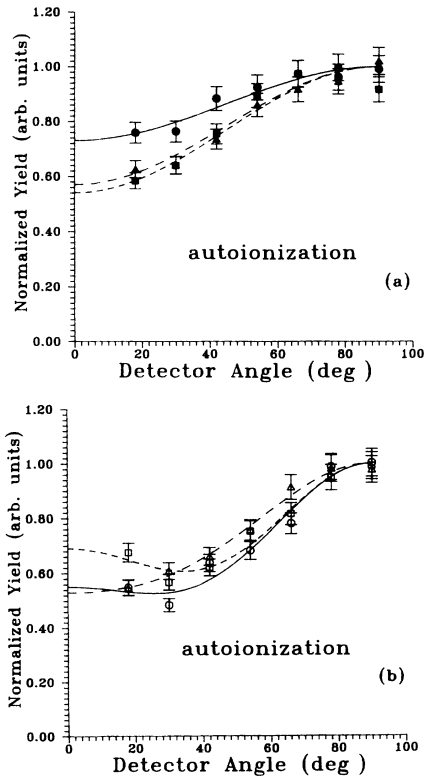

FIG. 7. Yield of H^+ ions from the autoinized state of H_2 as a function of the orientation of the molecular axis relative to the projectile direction. (a) electrons at 408 eV (●), 545 eV (▲), and 1089 eV (■); (b) protons at 0.75 MeV (○), 1.0 MeV (△), and 2.0 MeV (□). The smooth line is a fit to the data (see Table IV). The yields have been normalized at 90°.

The nondipole contribution to the interaction occurs in the single-collision process, while the double-collision process involves two dipole interactions.

The cross sections were expressed in the form of Eqs. (4) and (5) for fitting to the data. No attempt was made to separate first Born, second Born, and interference terms and investigate their angular dependence individually. In fact, if only s and p waves are considered, the angular dependence on θ_r expressed in Eq. (4) factors out of the first and second Born amplitudes.

It was pointed out in the Introduction that the calculations of Reading and Ford [15] showed the necessity of having a nondipole contribution in the collision in order for interference to occur between first and second Born amplitudes and produce the enhanced cross section for the negative projectile. It should be noted that the transition $1s\sigma_g^2 \rightarrow 2p\sigma_u k\sigma_g$ cited above as an example requires a dipole (σ_u) interaction in the collision when there is a single projectile-electron interaction (first Born), as in Figs. 1(a)–1(c), and has a nondipole contribution in the double-collision process (second Born) depicted in Fig. 1(d). The reverse is true for the transition $1s\sigma_g^2 \rightarrow 2p\sigma_u k\sigma_u$; the first Born amplitude is nondipole (σ_g) and the second Born amplitude has two dipole interactions. It is not possible in our experiment to tell if the nondipole contribution occurs in the first or second Born amplitudes.

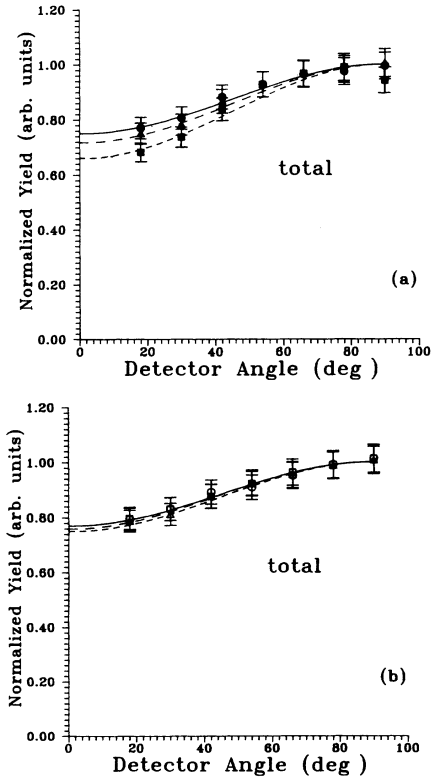

FIG. 8. Yield of H^+ ions from all states of H_2 as a function of the orientation of the molecular axis relative to the projectile direction. (a) electrons at 408 eV (●), 545 eV (▲), and 1089 eV (■); (b) protons at 0.75 MeV (○), 1.0 MeV (△), and 2.0 MeV (□). The smooth line is a fit to the data. The yields have been normalized at 90°.

IV. RESULTS

Expressions for $A(\theta_K)$ and $B(\theta_K)$ can be found [27] from the analysis given above. However, the experimental results are cross sections that have been integrated over all possible magnitudes and directions of the momentum-transfer vector K. Therefore, the values of A and B obtained from fitting the data to Eqs. (4) and (5), and listed in Tables II and III, represent averaged values rather than values at a particular K.

The first step in reducing the data is to fit [28] it to an expression of the form of Eq. (5). If the uncertainty in B, the coefficient in the $\cos^4\theta_r$ term, is greater than or approximately the same as B, then it is ignored [28] and Eq. (4) is used. A relative error of 5% for the data is used in the fitting routine which determines the coefficients and their uncertainties. The value of the reduced χ^2 of the fits are listed in Tables II and III as an indication of the scatter of the data.

Table IV lists the final states in accordance to the dependence of the cross section on the direction of the internuclear axis relative to the beam direction. Those showing the behavior of Eq. (4) are believed to be excited primarily by a dipole interaction while those showing the behavior of Eq. (5) have a large nondipole contribution. Figures 3–8 show the angular dependence of the cross sections. Error bars indicate a relative error of ±5%. All results have been normalized to unity at 90° to better display the angular dependence.

A. Double ionization

The doubly ionized state is represented in the tables as H^+H^+ and is listed in the column for excitations with large nondipole contributions. With the exception of the 1 MeV/amu electron-collision data, the angular distributions are close to being isotropic. This confirms earlier conclusions based on measurements of double-ionization cross sections measured at 30° and 90° for proton bombardment [29] and 45° and 90° for electron bombardment [20]. Similar results have been observed for low-energy proton collisions [30]. This nearly isotropic behavior could occur for collisions that are primarily dipole in nature with equal amounts of $k\sigma_u k'\sigma_g$ and $k\pi_u k'\sigma_g$ final states.

B. Ionization plus excitation

The collision process leading to a final state of a free electron and the H_2^+ ion in the $2p\sigma_u$ or $2s\sigma_g$ excited state appear to be predominantly dipole while those ending in the $2p\pi_u$ seem to have a large nondipole contribution. Based on the analysis presented here, there is no apparent reason why the $2p\pi_u$ channel should differ from the other two.

The H_2^+ $2s\sigma_g$ final state can be excited in a dipole interaction that leads to a final-state configuration of $2s\sigma_g k\sigma_u$ or $2s\sigma_g k\pi_u$ and equal contributions of each would lead to an isotropic distribution. This appears to be the case for electron bombardment where the angular distribution is close to isotropic.

C. Double excitation

The experimental procedure does not allow for any positive identification of the doubly excited terms produced in the collisions. Several states could and probably do contribute to the H^+-fragment yield in the 2–3 eV region and it is not known whether or not these states are dipole allowed. The electron-collision data indicates that dipole interactions dominate the collision process while the proton data suggests a larger nondipole contribution.

D. Comparison of projectiles

As was mentioned earlier, at the orientation of 90° the cross sections of two-electron processes for electron collisions is a factor of two or more greater than the same cross section produced by equivelocity proton collisions. The present data are consistent with this observation for all molecular orientation with one exception. In the case of the $2p\sigma_u$ final state, the ratio of electron to proton cross sections is closer to one at 0°. There is no indication as to why this occurs.

E. Final remarks

The energy dependence of the angular distributions is too complex to permit explanation. The velocity dependence of the coefficients A and B in Eqs. (4) and (5) depends on θ_K and, as stated earlier, θ_K cannot be inferred from the present data.

It is interesting to observe the behavior of the total H^+ yield observed in these measurements as shown in Figs. 8(a) and 8(b), rather than separating reaction channels. It should be noted that all channels involve two-electron processes. By considering the total yield, the uncertainties involved in decomposing the yield into subgroups is removed and the angular distributions are smoother and show less scatter.

For both electron and proton projectiles, the angular distributions are fit very well without a $\cos^4\theta$ term. Furthermore, the coefficients $A(\theta_K)$ of the $\cos^2\theta$ term are essentially the same for electrons and protons and show little or no energy dependence. These observations underline the dipole dominance of the collision processes.

ACKNOWLEDGMENT

This material is based upon work supported by the National Science Foundation under Grant No. PHY-9144420.

[1] H. K. Haugen, L. H. Andersen, P. Hvelplund, and H. Knudsen, Phys. Rev. A **26**, 1950 (1982).
[2] H. K. Haugen, L. H. Andersen, P. Hvelplund, and H. Knudsen, Phys. Rev. A **26**, 1962 (1982).
[3] H. Knudsen, L. H. Andersen, and P. Hvelplund, J. Phys. B **17**, 3545 (1984).
[4] M. B. Shah and H. B. Gilbody, J. Phys. B **18**, 899 (1985).
[5] L. H. Andersen, P. Hvelplund, H. Knudsen, S. P. Moller, K. Elsener, K.-G. Rensfelt, and E. Uggerhoj, Phys. Rev. Lett. **57**, 2147 (1986).
[6] R. D. DuBois and S. T. Manson, Phys. Rev. A **35**, 2007 (1987).
[7] L. H. Andersen, P. Hvelplund, H. Knudsen, S. P. Moller, A. H. Sorensen, K. Elsener, K.-G. Rensfelt, and E. Uggerhoj, Phys. Rev. A **36**, 3612 (1987).
[8] M. Charlton, L. H. Andersen, L. Brun-Nielsen, B. I. Deutch, P. Hvelplund, F. M. Jacobsen, H. Knudsen, G. Laricchia, M. R. Poulsen, and J. O. Pedersen, J. Phys. B **21**, L545 (1988).
[9] J. O. P. Pedersen and P. Hvelplund, Phys. Rev. Lett. **62**, 2373 (1989).
[10] J. O. P. Pedersen and F. Folkman, J. Phys. B **23**, 441 (1990).
[11] J. P. Giese, M. Schulz, J. K. Swensen, H. Schöne, M. Benhenni, S. L. Varghese, C. R. Vane, P. F. Dittner, S. M. Shafroth, and S. Datz, Phys. Rev. A **42**, 1231 (1990).
[12] J. H. McGuire, Phys. Rev. Lett. **49**, 1153 (1982).
[13] J. H. McGuire and J. Burgdörfer, Phys. Rev. A **36**, 4089 (1987).
[14] J. F. Reading and A. L. Ford, Phys. Rev. Lett. **58**, 543 (1987).
[15] J. F. Reading and A. L. Ford, J. Phys. B **20**, 3747 (1987); **21**, L685 (1988); **23**, 2567 (1990).
[16] R. E. Olson, Phys. Rev. A **36**, 1519 (1987).
[17] L. Végh, Phys. Rev. A **37**, 992 (1988); T. Watanabe and L. Végh, Nucl. Instrum. Methods B **40-41**, 89 (1989); L. Végh and J. Burgdörfer, Phys. Rev. A **42**, 655 (1990).
[18] J. H. McGuire and J. C. Straton, Phys. Rev. A **43**, 5184 (1991).
[19] N. Stolterfoht, in *High-Energy Ion-Atom Collisions,* edited by D. Berényi and G. Hock, Lecture Notes in Physics, Vol. 376 (Springer-Verlag, Heidelberg, 1991), p. 139.
[20] A. K. Edwards, R. M. Wood, A. S. Beard, and R. L. Ezell, Phys. Rev. A **37**, 3697 (1988).
[21] A. K. Edwards, R. M. Wood, J. L. Davis, and R. O. Ezell, Phys. Rev. A **42**, 1367 (1990); *ibid.* **44**, 797 (1991).
[22] L. H. Andersen, P. Hvelplund, H. Knudsen, S. P. Moller, J. O. P. Pedersen, S. Tang-Petersen, E. Uggerhoj, K. Elsener, and E. Morenzoni, J. Phys. B **23**, L395 (1990).
[23] N. Stolterfoht, Nucl. Instrum. Methods B **53**, 477 (1991).
[24] R. N. Zare, J. Chem. Phys. **47**, 204 (1967).
[25] C. J. Joachain, *Quantum Collision Theory* (North-Holland, Amsterdam, 1983).
[26] M. Weissbluth, *Atoms and Molecules* (Academic, New York, 1978).
[27] A. K. Edwards, R. M. Wood, M. W. Dittmann, J. F. Browning, M. A. Mangan, and R. L. Ezell, Nucl. Instrum. Methods B **53**, 472 (1991).
[28] P. R. Bevington, *Data Reduction and Error Analysis for the Physical Sciences* (McGraw-Hill, New York, 1969), Chap. 8.
[29] A. K. Edwards, R. M. Wood, and R. L. Ezell, Phys. Rev. A **31**, 99 (1985).
[30] B. G. Lindsay, F. B. Yousif, F. R. Simpson, and C. J. Latimer, J. Phys. B **20**, 2759 (1987).